CrystEngComm

Accepted Manuscript

ROYAL SOCIETY OF CHEMISTRY

www.rsc.org/crystengcomm

Journal Name

RSCPublishing

ARTICLE

Fabricating Roughened Surface on Halloysite Nanotubes via Alkali Etching for Deposition of High-Efficiency Pt Nanocatalysts

Cite this: DOI: 10.1039/xoxxooooox

Received ooth January 2012,
Accepted ooth January 2012

DOI: 10.1039/xoxxooooox

www.rsc.org/

Qiuru Wang, [a] Yanyan Wang, [a] Yafei Zhao, [a] Bing Zhang, [a,*] Yunyin, Niu, [a] Xu Xiang [b,*] and Rongfeng Chen [a]

Technological applications of heterogeneous nanocatalysts on supports have generally relied on the surface or interface properties of supports. Herein, we report a facile approach to fabricate roughened surface on halloysite nanotubes (HNTs) through etching the wall of HNTs in molten-salt system. SEM, TEM, XRD, FT-IR, AFM and N_2 adsorption/desorption analysis are employed to systematically investigate the morphology, structure and surface properties. Results suggest that roughness of HNTs surface has been significantly increased and defects are formed on the tube wall without structural damage. Subsequently the roughened halloysite nanotubes (RHNTs) are used as supports to prepare heterogeneous nanocatalyst. The Pt nanoparticles with uniform size can deposit homogeneously onto the RHNTs surface via one-step hydrothermal reduction. The as-prepared Pt@RHNTs catalyst exhibits remarkably improved activity and selectivity for hydrogenation of cinnamaldehyde towards cinnamyl alcohol compared with pristine halloysite support. Furthermore, Pt@RHNTs catalyst shows rapid catalytic rate in hydrogenation reaction and excellent leaching resistance in cycle uses.

1. Introduction

During the process of evolution of the earth, changeful natural environment had provided some suitable conditions for formation of natural nanomaterials. The silicate minerals, such as montmorillonite,[1] palygorskite[2] and halloysite,[3, 4] are pervasive compounds in the earth's crust and often exist in nano-size or present in various nano-morphologies. With the accompanied development of materials, the importance and value of natural nanomaterials in science have come to be acknowledged, which have the potential to be used as cheap alternatives to the expensive carbon nanotubes or other nanomaterials for the scale application.[5] Among these natural nanomaterials, halloysite ($Al_2Si_2O_5(OH)_4 \cdot 2H_2O$) with excellent physical-chemical properties, has been extensively investigated in different domains.[6-9] Halloysite nanotubes (HNTs) are naturally occurring aluminosilicate mineral with well-defined nanotubular structure, which consist of outside-in alternate silica tetrahedron sheet and alumina octahedron sheet in 1:1 stoichiometric ratio.[10-12] Due to their environmental friendliness and high chemical stability, HNTs have been recognized as fine lumens or supports to load bio-macromolecules and nanocatalysts.[13-15]

In the field of chemical industry, considering the separating difficulty and potential pollutions of homogeneous catalysts, the natural supports with nano-structure have attracted considerable interest of researchers for designing recoverable and environmentally friendly heterogeneous catalysts.[16] The common approach of preparing supported heterogeneous catalysts is to deposit[17-19]/graft[20] /coat[21, 22] catalysts onto certain supports, followed by post-treatment if necessary. However, as for HNTs, the tube walls exhibit low adhesion interaction with catalysts due to their surface smoothness and chemical inert of outer surface, which may result in difficulty loading, particle agglomeration and easily leaching from support surface.[15] Most often, organic functional modifiers and stabilizers (often polymer or ligands) are used to improve the surface properties of supports and strengthen the affinity for catalysts and other active components.[23, 24] Silylanization reaction [25, 26] and polymerization grafting[3, 7, 27] are commonly adopted for organic functionalization of halloysite nanotubes. However, these methods usually involve complicated operating processes. Additionally, these polymers are thereby unavoidably co-deposited onto the surface, and difficult to be removed completely, which may result in the performance degradation of catalysts. Thus, to find a cheap and flexible method to load nanocatalysts onto halloysite is critical for potential application. Surface science studies and density functional theory calculations[28, 29] illustrate that the supports' interfaces play an important role in the nanocatalysts creation and stabilization. Many technical applications of supports are enabled through the presence of rough surface with defects.[30-32] The existence of rough and defective surface can not only tune the properties of supports but also be involved directly as adsorption sites and active centers in chemical reactions in catalysis. Many previous researches have focused on fabricating the surface defects of carbon and other oxide nanomaterials in the

heterogeneous catalysis.[33, 34] However, to the best of our knowledge, similar research has not yet been performed on the surface of halloysite nanotube.

The molten-salt synthesis (MSS) method has been considered as a simple and cost-effective preparation approach of nano-powders.[35, 36] In the molten salt process, the molten salt can provide favorable flux environment with the solubility and diffusivity for solid-phase reaction, which can greatly reduce the synthesis temperature. Compared with solution synthetic method, the MSS doesn't require multiple steps and handling of large amounts of organic reagents, solvents and surfactants, and therefore reduces synthetic costs and environmental pollution. In the present study, we used this technique for achieving roughened and defective HNTs surface through alkali etching on the silica sheet of HNTs outer wall in molten-salt system, which was inspired by the etching phenomenon between strong alkali NaOH and SiO_2 materials at room temperature. In order to avoid excess etching by NaOH, we selected weak base Na_2CO_3 as etchant and combine $NaNO_3$ (molten point 308 °C) as molten agent to compose a molten-salt system at 350 °C. The solid etchant Na_2CO_3 dispersed in the $NaNO_3$ molten system can homogeneously react with HNTs walls and form soluble sodium salt in situ on the surface. The sample was washed with deionized water to remove soluble salts and to get roughened halloysite nanotubes (RHNTs) (Figure 1). The nanocatalysts of Pt were further deposited on the RHNTs to form Pt@RHNTs through a one-step hydrothermal process. The activity and selectivity of the as-prepared catalyst were also evaluated by hydrogenation of cinnamaldehyde (CAL) towards cinnamyl alcohol (COL).

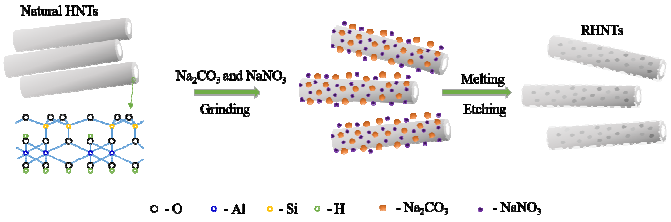

Figure. 1 Schematic illustration of the formation process of RHNTs.

2. Expetimental

2.1 Chemicals

Halloysite from Henan province in China was milled and sieved to obtain fine powders. Anhydrous sodium carbonate, sodium nitrate and ethylene glycol (EG) were purchased from Tianjin Fengchuan chemical reagent science and technology Co., Ltd. Hexachloroplatinic acid ($H_2PtCl_6 \cdot 6H_2O$, 99.9%) was obtained from Sinopharm chemical reagent Co. Ltd. (Shanghai, China). Trans-cinnamaldehyde (98.0%) was received from J&K Chemical Co. Ltd. Tetradecyl trimethyl ammonium bromide (TTAB) was from Aladdin reagent Co. Ltd. The experimental solution was prepared with deionized water. All chemicals were of analytical grade and used without further purification.

2.2 Preparation of Roughened Halloysite Nanotubes

A typical preparation of RHNTs included steps as follows: Firstly, 0.3 g of sodium carbonate and 5.0 g of sodium nitrate were grinded in an agate mortar, and 1.0 g of halloysite powder was subsequently added into the mixture and grinded continuously until three components were fully mixed. Secondly the mixed powder in a ceramic vessel was heated up to 350 °C in a tube furnace with a heating rate of 10 °C/min and kept for 2 hours in air. Then after cooling down, the sample was washed with deionized water for several times to remove soluble salts and impurities. Finally, the product was dried in a vacuum oven and indipink powder was obtained, marked as RHNTs.

2.3 Hydrothermal synthesis of Pt@RHNTs

Pt@RHNTs heterogeneous catalyst was synthesized through a facile hydrothermal process:[37, 38] 0.2 g of RHNTs were dispersed in 15 ml deionized water and 60 ml EG. Then 0.1035 g TTAB and 0.87 ml 0.0355 mol/L H_2PtCl_6 aqueous (3 wt% Pt loading ratio) were added into the suspension, followed by magnetic stirring for 2 h. Finally the obtained homogeneous solution were transformed into a 100 ml autoclave and heated at 120 °C for 4 h. The Pt@RHNTs sample was obtained by washing with ethanol and deionized water, followed by drying at 50 °C for 12 h. In order to compare RHNTs with natural HNTs as supports, Pt@HNTs was synthesized in the same procedure.

2.4 Catalytic performance testing and Reuse of catalysts

Selective hydrogenation of cinnamaldehyde was carried out in a 100 ml stainless autoclave connected with a hydrogen cylinder to evaluate the catalytic performance of Pt@RHNTs and Pt@HNTs. A typical catalytic process was shown as follows:[39, 40] In the autoclave with a Teflon inner layer, 50 mg catalysts (Pt@RHNTs or Pt@HNTs) and 4 mmol cinnamaldehyde was dispersed in 15 ml solvent ethanol. The catalytic reactor was purged with H_2 (2 MPa) for 10 cycles. After preheating without H_2, the reactor was sealed with 1 MPa H_2 and heated in 60 °C bath with magnetic stirring at 720 rpm for a certain time. When the catalytic reaction was finished, the catalysts were collected by centrifugation and washing with ethanol for three times, followed by a drying process at 50 °C for 12 h. Then they were used for the next catalytic reaction in the same conditions above.

2.5 Characterizations

The morphology and dimension of samples were observed by the scanning electron microscopy (SEM, JSM-6701F) and transmission electron microscope (TEM, Tecnai G2 20). X-ray diffractometer (XRD, D8ADVANCE) with the 2θ range of 5-80 ° and Fourier transformed infrared spectroscopy (FT-IR, Varian 800) scanning from 400 to 4000 cm^{-1} were employed to analyze structures of RHNTs and HNTs. Atomic force microscope (AFM, Dimension FastScan) were used to observe the surface of the samples by using a mica substrate. BET surface area and BJH pore size distributions of the samples were obtained by using the GEMINI VII2390 surface area and pore size analyzer. Inductively coupled plasma atomic emission spectroscopy (ICP-AES, Shimadzu ICPS-7500) was employed to conduct elemental analysis and determine Pt loading capacity on supports. The products of hydrogenation reaction were analyzed through a gas chromatograph (GC-9800) with a capillary column (Agilent, DB-624) using a flame ionization detector (FID).

3. Result and discussions

3.1 Characterizations of HNTs and RHNTs

SEM and TEM characterizations. SEM and TEM images of HNTs and RHNTs are presented in Figure 2, exhibiting the morphology and size of the samples. As shown in Figure 2a, the HNTs possess natural open-ended tubular morphology with external diameters in the range of 50-70 nm and the average length of 500 nm. Figure 2b further reveals the hollow tube structure with an inner diameters about 15-30 nm. Moreover, both SEM and TEM images in Figure 2a and 2b show smooth and flat surface of HNTs. Figure 2c and 2d present the morphology of as-prepared RHNTs, from which one can observe that the size of the nanotubes remain unchanged and preserved original geometry. However, in contrast with HNTs, surfaces variations occur on RHNTs after etching. It can be seen from SEM image in Figure 2c that each nanotube exhibits rough surface, with hackly edges on the outer walls. TEM image in Figure 2d further reveals that defects are formed on the surface of RHNTs and result in the roughening of outer walls, which is consistent with the result of SEM analysis. Therefore, comparison between morphology of natural and etching samples confirms the successful preparation of roughened halloysite with defective surface. The EDS spectra reveal that the nanotubes is mainly composed of Al, Si and O, and the average atomic ratios of Al to Si in HNTs and RHNTs, within the experimental limit, are both close to 1:1, which indicated that silica in outer surface and alumina in inner surface were etched by sodium carbonate simultaneously by salt-molten method. The etching on outer and in inner surface of nanotubes could increase its surface area correspondingly.

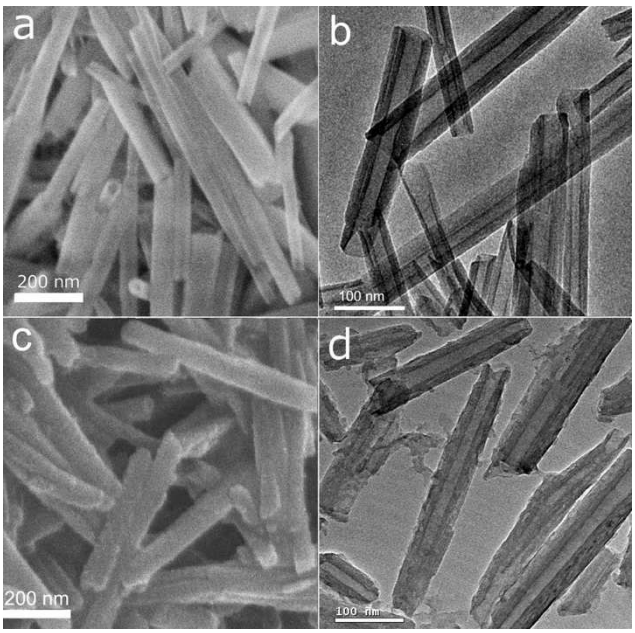

Figure. 2 (a) SEM and (b) TEM images of HNTs, (c) SEM and (d) TEM images of RHNTs.

XRD and FT-IR analysis. Figure 3 displays the X-ray diffraction patterns of HNTs and RHNTs. In XRD pattern of HNTs, all of the observed peaks can be indexed to the characteristic peaks of halloysite (7 Å) (JCPDS card No. 09-0453). The peak appearing at 2θ of 11.79° (d_{001}=7.5 Å) corresponds to the multilayer wall packing.[11] The sharp peak at 2θ of 20.07° (d_{100}=4.42 Å) is ascribed to another characteristics of tubular halloysite. Peaks of RHNTs agree well with that of natural halloysite except for the relative intensity decreasing of peaks at 11.79° and 20.07°, indicating that layered character and tube wall crystallinity are partially weaken, which is probably due to etching occurring on the wall of nanotubes. Thus it is further confirmed that RHNTs not only possess the same crystal phase with HNTs but also exhibit similar tube wall structural characters, which is corresponding to the results from morphology analysis.

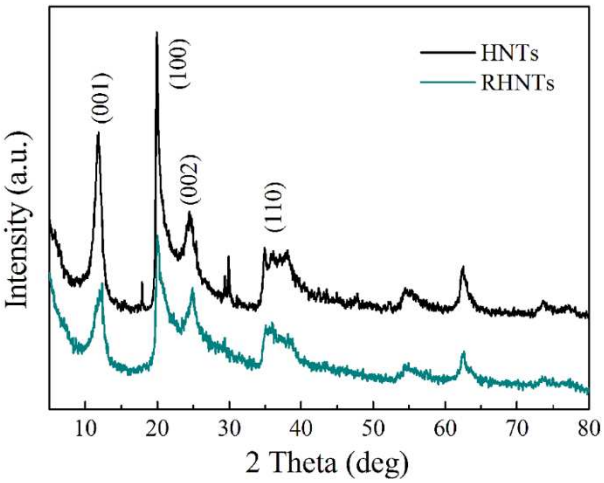

Figure. 3 XRD patterns of HNTs and RHNTs.

The FT-IR mesurement was employed to investigate the composition and structure of HNTs and RHNTs samples. As shown in Figure 4, there is no significant change in the spectrum of RHNTs compared with HNTs. Both have same composition features: such as the absorption peak of Si–O bending vibration at 531 cm^{-1}, peak at 466 cm^{-1} ascribed to Al–O stretching mode and peak corresponding to the Si-O-Al perpendicular stretching at 753 cm^{-1}. However, the peaks of Al-OH bending vibration (911 cm^{-1}) and stretching vibration (3625 cm^{-1} and 3698 cm^{-1}) present trend of decrease in different degrees, which results from that etching partly on the wall has an influence on the chemical bond between silica tetrahedron sheet and alumina octahedron sheet and lead to the loss of O-H groups.

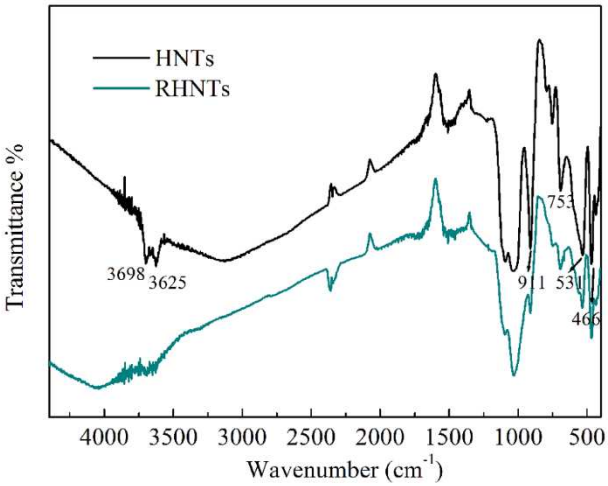

Figure. 4 FT-IR spectra of HNTs and RHNTs.

AFM and N_2 adsorption/desorption analysis. To further investigate the variations of surface properties, HNTs and

RHNTs were characterized by atomic force microscope (AFM) analysis. The 2D images of the natural and roughened samples with scan sizes of 0.5 μm × 0.5 μm are given in Figure 5, showing a comparison of the surface morphology of HNTs and RHNTs. It can be observed in Figure 5a that HNTs are endowed with smooth edges, while RHNTs with rough and irregular edges in Figure 5b, which is in accordance with the results of SEM and TEM analysis. The surface roughness parameters, generally expressed in terms of the mean roughness (Ra) and the root mean square roughness (Rq), are calculated from the 2D images with same size of selected areas by using NanoScopeAnalysis from Bruker Company. Both Rq and Ra of RHNTs have higher values (Rq=2.80 nm, Ra=2.32 nm) than those of HNTs (Rq=0.760 nm, Ra=0.624 nm), showing a remarkably increasing by 3 times. The formation of highly roughened surface may provide a more favorable deposition environment on carrier surface for active nanoparticles and provide potential active sites in catalytic reaction.

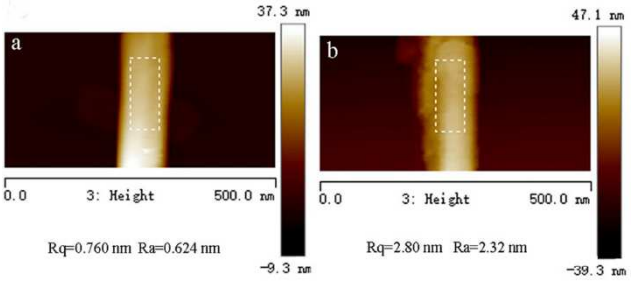

Figure. 5 AFM images of (a) HNTs, (b) RHNTs.

In addition, nitrogen adsorption analyses were also conducted to study the changes in surface properties. Figure 6 presents the Nitrogen adsorption–desorption isotherms of HNTs and RHNTs. Both of the isotherms, exhibiting similar patterns, belong to type IV with H3 hysteresis loops according to the basis of IUPAC recommendations. The results are accordant with the category of cylindrical pore, further indicating that the prepared RHNTs keep tubular morphology. Calculated from the isotherms by using BET method, the specific surface area of HNTs and RHNTs are 44.98 $m^3 \cdot g^{-1}$ and 51.07 $m^3 \cdot g^{-1}$, respectively, presenting a slight through etching. In the pore size distribution curves, RHNTs and HNTs exhibit similar distributions. However, for RHNTs an extra pore size distribution appears at 3-4 nm, corresponding to a few of mesopores forming on the surface of RHNTs etched by Na_2CO_3.

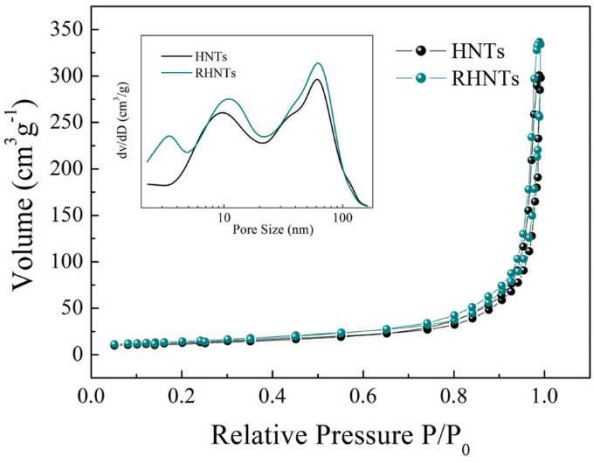

Figure. 6 (a) Nitrogen adsorption–desorption isotherms of HNTs and RHNTs, (b) pore size distributions of HNTs and RHNTs.

3.2 Characterizations of Pt@HNTs and Pt@RHNTs

In order to study the performance of RHNTs for nanocatalysts deposition and dispersion, Pt was selected in this work to prepare heterogeneous catalysts. The as-prepared Pt@RHNTs and Pt@HNTs were evaluated by transmission electron microscopy, and the images are clearly shown in Figure 7. It can be observed from Figure 7a, few Pt particles deposit on the exterior surface or interior lumen of natural HNTs. There are a large number of particles aggregated beside the nanotubes. In stark contrast to natural halloysite, a great quantity of colloidal Pt nanoparticles with uniform size are homogeneously decorated on the surface of RHNTs (Figure 7b). ICP-AES was applied to determine Pt loading capacity on both RHNTs (2.49 wt%) and HNTs(1.45 wt%), further confirming that the roughened surface is beneficial to deposit Pt catalyst on RHNTs than natural HNTs. Moreover, the size distribution of nanoparticles was estimated by software of Nano Measurer in Figure 7d, which exhibits a relative narrow particle size distribution from 3 to 5 nm with an average diameter of 3.8 nm. Through the comparison between Pt@RHNTs and Pt@HNTs, it can be concluded that the Pt catalysts are more liable to be loaded onto RHNTs with higher dispersion, which could be ascribed to two reasons as following: (1) In spite of slightly increased surface area, remarkably improved surface roughness may play an important role and greatly enhance the adsorption capacity for precursor of Pt catalyst; (2) surface defects forming on the support can play a role of nucleation centers and favor the growth of the catalyst particles.[31, 41] The increased dispersibility and higher loading capacity could enhance the specific surface area (61.07 $m^3 \cdot g^{-1}$) of catalyst Pt@RHNTs compared with specific surface area (48.39 $m^3 \cdot g^{-1}$) of Pt@HNTs, and would accordingly improve the catalytic performance.The increased dispersibility would highly enhance the whole specific surface area of catalyst and accordingly improve the catalytic performance. Additionally, HRTEM observation (Figure 7c) give an insight into Pt nanoparticles decorated on RHNTs. It suggests that the lattice fringes with a spacing of 0.223 nm are clearly visible in Pt nanoparticles on RHNTs, which is consistent with the d-spacing of the (111) planes of Pt. Studies have proved that hexagonal Pt (111) has great advantages for selectively hydrogenation of C=O in unsaturated aldehyde over Pt (100) and polycrystalline Pt.[38]

The catalysts of Pt/HNTs and Pt/RHNTs were also characterized by temperature programmed reduction of hydrogen (H_2-TPR) to investigate the interaction between Pt particles and supports. There is a very weak peak for the reduction curve of Pt/HNTs and Pt/RHNTs at 249°C and 302°C, respectively. Compared with reduction temperatures, the nanoparticles on RHNTs are more difficult to reduce, which show that interaction between Pt particles and RHNTs is stronger than that of Pt particles and HNTs. Furthermore, the reduction temperature of nanoparticles on RHNTs is higher than that of other HNT supported metal catalysts.[42] The reason can be partially attributed that the roughened surface of RHNTs can improve bonding strength between Pt particles and RHNTs

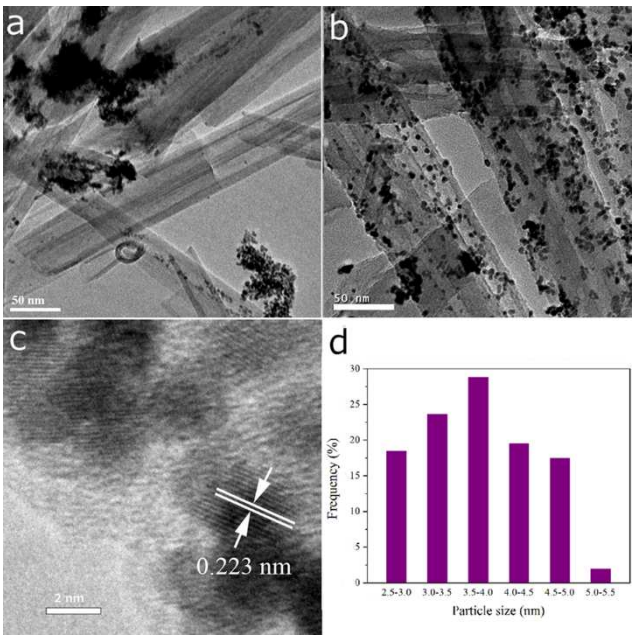

Figure. 7 TEM images of (a) Pt@ HNTs and (b) Pt @RHNTs, (c) HRTEM image of Pt @RHNTs and (d) particle size distribution gram of Pt @RHNTs.

3.3 Catalytic performance studies

Selective hydrogenation of α, β-unsaturated aldehydes to unsaturated alcohols is of great significance for producing various fine chemicals, pharmaceutical intermediates and for scientific insight of catalyst design. Selective hydrogenation of cinnamaldehyde (CAL) to cinnamyl alcohol (COL) is a representative of such a class of reactions. Many published researches have applied Pt catalysts for selective hydrogenation of CAL to COL.[40, 41] In present work, catalytic hydrogenation test of CAL was carried out to study the performance of Pt@RHNTs. In contrast, catalytic test was also conducted by using Pt@HNTs as catalyst. Figure 8a presents the effects of time on conversion and selectivity of catalytic hydrogenation for both catalysts. It can be seen that Pt@RHNTs catalyst exhibits higher efficiency for CAL hydrogenation. At the initial stage of reaction (within 5 min), the conversion and C=O selectivity rapidly reach 93.02% and 83.39%, respectively. Then the reaction rate slow down until the reactant is almost completely converted within 30 min. In the meantime, selectivity decrease gradually during the process due to the formation of complete hydrogenation product hydrocinnamyl alcohol (HCOL). Compared with Pt@RHNTs, the CAL conversion and selectivity for COL of Pt@HNTs are 49.03% and 68.78% at 5 minutes, respectively, which maintain a low level within 30 min. Both CAL conversion and COL selectivity of Pt@RHNTs are much higher than those of Pt@HNTs. This can be ascribed to the improving dispersion and growing loading content of Pt nanoparticles on RHNTs, thus exposing more active sites for catalytic reaction.

The conversion, selectivity and turnover frequency (TOF, defined as moles of converted CAL per mole of exposed Pt per seconds) are listed in Table 1 to further estimate the catalytic activity of Pt@RHNTs and other Pt-based catalysts. The conversion of Pt@RHNTs catalyst is as high as 93.02% with a high C=O selectivity of 83.39% within 5 min, showing a far more fast and efficient catalytic process compared with other Pt-based catalysts for hydrogenation of cinnamaldehyde. Additionally, the reaction can be fulfilled at a more mild condition (60 ℃, 1 Mpa) by using Pt@RHNTs catalyst. The TOF of Pt@RHNTs can reach 3.6 s^{-1}, highest than that of most Pt catalysts on other supports in the literatures. Such a high catalytic efficiency can be viewed from the perspective of reaction kinetics: (1) Similar to other porous catalyst supports,[43, 44] RHNTs have a large specific surface area, roughened surface and a porous nanostructure with accessibility to external reagents, and accelerate nano-platinum catalytic reactions. (2) The synergetic catalysis effect between the anchored catalyst atoms and surface defects can improve catalytic efficiency, providing beneficial conditions for faster activation of reactants. (3)The roughened surface of RHNTs, with effects similar to the specific tubular structure,[45] could immobilize the Pt nanocatalyst firmly and protect against particle agglomeration. It can be concluded that the support especially the surface property of the support is of great importance to improve catalytic performance and play an important role in heterogeneous nanocatalysts.[44, 28]

Figure 8b shows the recyclability of the Pt@RHNTs catalytic composite for 5 cycles. Throughout five reuses, the CAL conversion and selectivity for COL over Pt@RHNTs almost do not decrease but maintain high level, which are still above 90% and 80%, respectively. After 5 cycle uses, Pt loading amount (2.34 wt%) of Pt@RHNTs only decrease by 6% compared with initial value(2.49 wt%), exhibiting an excellent leaching resistance. It suggests that the rough surface of RHNTs indeed strengthen the interaction between nanocatalyst and support, contributing significantly to anchor nanoparticles and protecting them from leaching in cycle use.

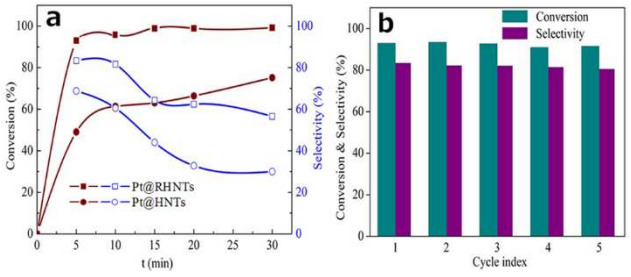

Figure. 8 (a) Conversion and selectivity of Pt@HNTs and Pt @RHNTs for product cinnamyl alcohol as a function of reaction time. (b) Recyclability of the Pt @RHNTs.

4. Conclusions

In summary, roughened halloysite nanotubes have been fabricated through simple etching process by using sodium carbonate as etchant in molten-salt system. It was confirmed

that roughened surface with defects had been formed on the tube wall and the surface roughness of RHNTs increased remarkably, as well as BET surface area. With improved surface properties, Pt catalysts were more liable to deposit on the surface of RHNTs with a narrow diameter distribution and higher dispersion than HNTs as support. The as-prepared Pt@RHNTs catalyst showed highly improved activity and selectivity of for selective hydrogenation of cinnamyl aldehyde compared with Pt@RHNTs, which were as high as 93.02% and 83.39% respectively within 5 min. The heterogeneous catalyst also exhibited higher catalytic rate and superior recoverability. It was convinced that roughness and defects of RHNTs surface played critical roles both in loading process of Pt particles and catalytic reaction process. It is expected that RHNTs could be of great potential as a promising support material for not only catalytic field, but also for a wide applications such as pharmacology research and environmental protection.

Table. 1 Catalytic activity of different supported Pt-based catalysts for hydrogenation of cinnamaldehyde.

Catalysts	Conversion (%)	Selectivity (%)	TOF (s^{-1})	Reaction conditions
Pt@RHNTs	93.0	83.4	3.6	60 ℃, 1 Mpa, 5 min
Pt/RGO[39]	73.9	83.2	0.445	70 ℃, 2 Mpa, 2 h
Pt/AC[39]	20.1	70.3	0.122	70 ℃, 2 Mpa, 2 h
Pt/SiO_2-NH_3[44]	15	12	0.03	150 ℃, 1Mpa,2 h
Pt/SiO_2-Sigma[44]	18	40	0.24	150 ℃, 1Mpa, 2 h
Pt/MA-1[46]	79.7	85.4	0.488	60 ℃, 1 Mpa, 2 h
Pt/MA-2[46]	84.3	76.6	0.410	60 ℃, 1 Mpa, 2 h
Pt/CeO_2-ZnO_2[48]	42.3	97.3	0.34	25℃, 2 Mpa, 8 h
Pt/CA-LiH973[49]	50	53	3.5	90 ℃, 1 Mpa, 26.8 min

Acknowledgements
This work was supported by the National Natural Science Foundation of China (Grants 21271158 and 21076016).

Notes and references
[a] School of Chemical Engineering, Zhengzhou University, Zhengzhou 450001, People's Republic of China.
E-mail: zhangb@zzu.edu.cn
[b] State Key Laboratory of Chemical Resource Engineering, Beijing University of Chemical Technology, Beijing 100029, People's Republic of China
E-mail: xiangxu@mail.buct.edu.cn.

1 J. Xiong, C. Hang, J. Gao, Y. Guo and C. Gu, *Chem. Eng. J.*, 2014, **254**, 276.
2 A. A. Aghzzaf, B. Rhouta, E. Rocca, A. Khalil, C. Caillet and R. Hakkou, *Mater. Chem. Phys.*, 2014, **148**, 335.
3 W. O. Yah, H. Xu, H. Soejima, W. Ma, Y. Lvov and A. Takahara, *J. Am. Chem. Soc.*, 2012, **134**, 12134.
4 W. O. Yah, A. Takahara and Y. Lvov, *J. Am. Chem. Soc.*, 2012, **134**, 1853.
5 R. Zhai, B. Zhang, L. Liu, Y. D. Xie, H. Q. Zhang and J. D. Liu, *Catal. Commun.*, 2010, **12**, 259.
6 G. Cavallaro, G. Lazzara, S. Milioto, F. Parisi and V. Sanzillo, *ACS Appl. Mater. Inter.*, 2014, **6**, 606.
7 G. Cavallaro, D. I. Donato, G. Lazzara and S.Milioto, *J. Phys. Chem. C.*, 2011, **115**, 20491.
8 S. Barrientos-Ramírez, G. M. Oca-Ramírez, E. V. Ramos-Fernández, A. Sepúlveda-Escribano, M. M. Pastor-Blas and A. González-Montiel, *Appl. Catal. A.*, 2011, **406**, 22.
9 J. Liang, Z. Fan, S. Chen, S. Ding and G. Yang, *Chem. Mater.*, 2014, **26**, 4354.
10 E. Abdullayev and Y. Lvov, *J. Mater. Chem. B.*, 2013, **1**, 2894.
11 E. Abdullayev, A. Joshi, W. B. Wei, Y. F. Zhao and Y. Lvov, *Acs Nano.*, 2012, **6**, 7216.
12 P. Luo, Y. F. Zhao, B. Zhang, J. D. Liu, Y. Yang and J. F. Liu, *Water Res.*, 2010, **44**, 1489.
13 C. Chao, B. Zhang, R. Zhai, X. Xiang, J. D. Liu and R. F. Chen, *ACS Sustainable Chem. Eng.*, 2014, **2**, 396.
14 R. Zhai, B. Zhang, Y. Z. Wan, C. C. Li, J. T. Wang and J. D. Liu, *Chem. Eng. J.*, 2013, **214**, 304.
15 Y. Lvov and E. Abdullayev, *Prog. Polym. Sci.*, 2013, **38**, 1690.
16 Y. Zhang, Y. Xie, A. Tang, Y. Zhou, J. Ouyang and H. Yang, *Ind. Eng. Chem., Res.* 2014, **53**, 5507.
17 N. I. Andersen, A. Serov and P. Atanassov, *Appl. Catal. B.*, 2015, **163**, 623.
18 Y. Lei, B. Liu, J. Lu, R. J. Lobo-Lapidus, T. Wu, H. Feng, X. Xia, A. U. Mane, J. A. Libera, J. P. Greeley, J. T. Miller and J. W. Elam, *Chem. Mater.*, 2012, **24**, 3525.
19 T. Dobbelaere, A. K. Roy, P. Vereecken and C. Detavernier, *Chem. Mater.*, 2014, **26**, 6863.
20 R. Ghorbani-Vaghei, S. Hemmati and H. Veisi, *J. Mol. Catal. A: Chem.*, 2014, **393**, 240.
21 L. Wang, J. Chen, L. Ge, V. Rudolph and Z. Zhu, *J. Phys. Chem. C.*, 2013, **117**, 4141.
22 J. Bravo, A. Karim, T. Conant, G. P. Lopez and A. Datye, *Chem. Eng. J.*, 2004, **101**, 113.
23 S. B. Hartono, M. Yu, W. Gu, J. Yang, E. Strounina, X. L. Wang, S. Z. Qiao and C. Z. Yu, *Nanotechnology.*, 2014, **25**, 1.
24 M. R. Karim, Y. Ikeda, T. Ide, S. Sugimoto, K. Toda, Y. Kitamura, T. Ihara, T. Matsui, T. Taniguchi, M. Koinuma, Y. Matsumoto and S. Hayami, *New J. Chem.*, 2014, **38**, 2120.
25 L. N. Carli, T. S. Daitx, G. V. Soares, J. S. Crespo and R. S. Mauler, *Appl. Clay Sci.,* 2014, **87**, 311.
26 H. Zhu, M. L. Du, M. L. Zou, C. S. Xu and Y. Q. Fu, *Dalton Trans.*, 2012, **41**, 10465.
27 H. X. Yu, Y. T. Zhang, X. B. Sun, J. D. Liu and H. Q. Zhang, *Chem. Eng. J.*, 2014, **237**, 322.
28 D. S. Su, S. Perathoner and G. Centi, *Chem. Rev.*, 2013, **113**, 5782.
29 F. Yang, Y. Choi, P. Liu, D. Stacchiola, J. Hrbek amd J. A. Rodriguez, *J. Am. Chem. Soc.*, 2011, **133**, 11474.
30 Y. S. Yun, G. Yoon, K. Kang and H. J. Jin, *Carbon.*, 2014, **80**, 246.

31 Z. Huang, Z. Luo, Y. V. Geletii, J. W. Vickers, Q. Yin, D. Wu, Y. Hou, Y. Ding, J. Song, D. G. Musaev, C. L. Hill and T. Lian, *J. Am. Chem. Soc.*, 2011, **133**, 2068.

32 K. Katsiev, M. Batzill, L. A. Boatner and U. Diebold, *Surf. Sci.*, 2008, **602**, 1699.

33 Y. De-Quan and E. Sacher, *J. Phys. Chem. C.*, 2008, **112**, 4075.

34 L. Giordano, C. Di Valentin, G. Pacchioni and J. Goniakowski, *Chem. Phys.*, 2005, **309**, 41.

35 Y. Ki Hyun, C. Yong Soo and K. Dong Heon, *J. Mater. Sci.*, 1998, **33**, 2977.

36 Y. K. Liu, C. L. Zheng, W. Z. Wang, C. R. Yin and G. H. Wang, *Adv. Mater.*, 2001, **13**, 1883.

37 S. H. Hsieh, M. C. Hsu, W. L. Liu and W. J. Chen, *Appl. Surf. Sci.*, 2013, **277**, 223.

38 Y. F. He, J. T. Feng, Y. Y. Du and D. Q. Li, *ACS Catal.*, 2012, **2**, 1703.

39 J. J. Shi, R. F. Nie, P. Chen and Z Y. Hou, *Catal. Commun.*, 2013, **41**, 101.

40 Z. Rong, Z. Sun, Y. Wang, J. Lv and Y. Wang, *Catal. Lett.*, 2014, **144**, 980.

41 L. Giordano, G. Pacchioni, F. Illas and N. Rösch, *Surf. Sci.*, 2002, **499**, 73.

42 L. Wang, J. Chen, L. Ge, Z. H. Zhu, V. Rudolph, *Energy Fuels*, 2011, **25**, 3408.

43 G. Zhang, S. Sun, M. Cai, Y. Zhang, R. Li and X. Sun, *Sci Rep.*, 2013, **3**, 1038.

44 X. Peng, J. Chen, J. A. Misewich and S. S. Wong, *Chem. Soc. Rev.*, 2009, **38**, 1076.

45 N. Sanchez-Ballester, G. Ramesh, T. Tanabe, E. Koudelkova, J. Liu, L. K. Shrestha, Y. Lvov, J. P. Hill, K. Ariga, H. Abe, *J. Mater. Chem.*, **2015**, DOI: 10.1039/C4TA06966H.

46 K. Q. Sun, Y. C. Hong, G. R. Zhang and B. Q. Xu, *ACS Catal.*, 2011, **1**, 1336.

47 X. Xiang, W. He, L. Xie and F. Li, *Catal. Sci. Technol.*, 2013, **3**, 2819.

48 S. Bhogeswararao and D. Srinivas, *J. Catal.*, 2012, **285**, 31.

49 B. F. Machado, S. Morales-Torres, A. F. Pérez-Cadenas, F. J. Maldonado-Hódar, F. Carrasco-Marín, A. M. T. Silva, J. L. Figueiredo and J. L. Faria, *Appl. Catal. A*., 2012, **425-426**, 161.

Table of Contents Graphic

Roughened halloysite nanotubes (RHNTs) were fabticatied through etching the wall of HNTs in molten-salt system.